Defect modes in a stacked structure of chiral photonic crystals

Jiun-Yeu Chen and Lien-Wen Chen*
Department of Mechanical Engineering, National Cheng Kung University, 1, Ta-Hsueh Road, Tainan 701, Taiwan
(Received 27 December 2004; published 22 June 2005)

An optical propagation simulation is carried out for the study of photonic defect modes in a stacked structure of cholesteric liquid crystal films with spatially varying pitch. The defects are introduced by a pitch jump and a phase jump in the cholesteric helix. The effect of a finite sample thickness on transmission of the defect mode and on the required polarization of incident light to create the defect mode is discussed. For normal and near-normal incidence of circularly polarized light with the same handedness as structure, the defect caused by a pitch jump results in discrete peaks within a forbidden band in the transmission. The particular spectrum is similar to the feature of a Fabry-Pérot interferometer. By introducing an additional phase jump, linear blueshifts of the defect modes in transmission spectra are correlated with an increase in the twist angle.

DOI: 10.1103/PhysRevE.71.061708 PACS number(s): 42.70.Df, 42.70.Qs, 61.30.−v

I. INTRODUCTION

Materials having an ordered structure with a spatially periodic dielectric constant, called photonic band-gap (PBG) materials, have attracted much interest from both fundamental and practical viewpoints [1]. The primary reason is the fact that the PBG in which no electromagnetic mode exists can be realized in such materials. For the medium with a periodicity on the order of the optical wavelength, the physical phenomena of the PBG have been theoretically predicted and considerable research has been proposed, especially in the study of a localized defect mode within the stop band. The localization of light is generated and a defect mode emerges within the forbidden band when a disorder is introduced to the periodic dielectric structure [2,3]. The feature of the strongly localized eigenstates of photons can be applied to optical microcircuits, narrow band filters, and lasers with low thresholds [4,5].

Although the one-dimensional photonic crystals (PCs) do not have a complete PBG as the three-dimensional PCs do, a benefit is the ease of fabrication and introduction of defects for applications in the range of the visible light wavelength. A cholesteric liquid crystal (CLC), which has a self-organized chiral structure with a periodicity of the optical wavelength, can be regarded as a one-dimensional PC. In their Grandjean texture, the directors of liquid crystal molecules lie homogeneously in the plane perpendicular to the helical axis and rotate continuously along the axis. The CLC shows a photonic stop band for the circularly polarized light with the same handedness as the helix propagating along a helical axis. The selective reflection is of great interest for display applications [6], and the laser action at the edge of a PBG, where the photon group velocity approaches zero, can be used for producing microlasers and photonic devices [7,8]. Liquid crystals have a large optical anisotropy so that some degree of tunability in the band structure can be obtained by electro-optic effects [9]. For active laser devices, the combination with photoreactive CLC materials also provides the advantage of the tunable PBG during operation [10].

The introduction of the defect into the chiral structure of CLCs has been also discussed. In numerical simulations, a defect can be created by inserting an optically isotropic layer in a CLC [11]. By the discontinuity in the helix, the twist defect gives rise to the localized modes at the position of the defect [12,13]. For the two kinds of defects and the combination of both, all of the induced defect modes reveal a sharp dip or peak in simulated reflection/transmittance curves for both circular polarizations of incident light [14]. An alternative way to generate photonic defect modes is the modulation of helical twisting power (HTP) [15,16]. Both of the local and global deformations in the helix could induce the localized modes in the forbidden band. The essential difference in this method is that the defect modes appear only for the incident circular light with the same handedness as the cholesteric screw.

By varying the lattice repeat distance, photonic structures can be made to vary spatially. For the CLCs with spatially varying pitch, solid structures are needed to stabilize the pitch gradient. With the photochemical reaction of liquid-crystal monomers [17] or a thermal diffusion in a glassy CLC [18], it is possible to freeze-in the mesophases into stable polymetric structures or to quench cholesteric liquid crystalline oligomers from the glassy state to the solid. The spatially varying photonic structure can provide a wider range of the photonic stop band than a uniform arranged texture. Optical properties of wideband CLCs have been used in wideband reflectors and reflective polarizers for display devices [6,19].

In the present research, the variable pitch cholesterics are assumed to explore whether the introduction of the defects has any utility and what limitations originate. The gradient pitch is assumed to have an exponential profile. The defects are introduced by a pitch jump and a helical phase jump. The model is a stacked structure of two CLC films with spatially varying period. The control of defect mode wavelengths is investigated theoretically, and the defect modes related to the configuration are studied to understand the effect of the modification of HTP. The numerical treatment is based on

*Corresponding author. FAX: 886-6-2352973. Email address: chenlw@mail.ncku.edu.tw

the Galerkin finite element method (FEM) [20]. Moreover, the spatially varying pitch of a CLC can be performed by thermal treatment or photoinduced diffusion, so that the model of calculation can be considered as a realizable concept.

II. MODEL AND METHOD OF ANALYSIS

The helix deformation in a CLC can be described by a power series [17] or an exponential form [19]. In the analysis presented, the planar structure of a single CLC film as shown in Fig. 1(a) is assumed to have an exponentially varying pitch $P(z)$. Along the helical z axis, the pitch distribution function can be expressed as

$$P(z) = P_{\min} \exp\left(\frac{z}{d} \ln \gamma\right), \tag{1}$$

where d is the thickness of a single CLC film, and γ is the ratio of the largest and the smallest pitch ($P_{\max}/P_{\min}$). In order to analyze the optical properties of the defect modes by introduction of a pitch jump and a helical phase jump into a CLC with spatially varying pitch, the model as shown in Figs. 1(b) and 1(c) is carried out by stacking the CLC films in Fig. 1(a). The transmission characteristics of the employed one-dimensional PC structure are solved by the Galerkin FEM. The Maxwell equations can be used to analyze the light propagation in the medium with refractive index varying along the propagating direction [20,21]. The equation of light propagation with angular frequency ω is given by Berreman [22]:

$$\frac{d\mathbf{\Psi}(z)}{dz} = \frac{i\omega}{c}\mathbf{D}(z)\mathbf{\Psi}(z), \tag{2}$$

where $\mathbf{\Psi}(z)$ is the field vector expressed as $\mathbf{\Psi}(z) = (E_x, H_y, E_y, -H_x)^T$, and $\mathbf{D}(z)$ is the differential propagation matrix. The important parameters to determine the CLC characteristics are the dielectric constants $\varepsilon_{\parallel}$ and $\varepsilon_{\perp}$ in the principal axes. Defining $\varepsilon \equiv (\varepsilon_{\parallel} + \varepsilon_{\perp})/2$ and $\delta \equiv (\varepsilon_{\parallel} - \varepsilon_{\perp})/2$, the wave equations for the electric field $\mathbf{E}$ can be derived from Eq. (2) by eliminating the magnetic field $\mathbf{H}$:

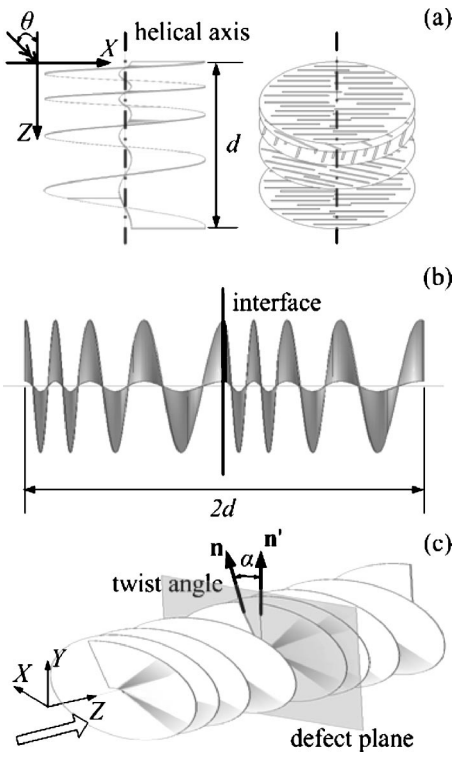

FIG. 1. Schematic views of chiral structures with gradient pitch length. (a) A single CLC film with spatially varying pitch. The film thickness and the oblique incident angle of light are d and θ, respectively. (b) A pitch jump is introduced into the cholesteric helix. (c) A pitch jump plus a helical phase jump with a twist angle α. $\mathbf{n}$ and $\mathbf{n}'$ are the nematic directors. The open arrow indicates the light propagating direction.

$$\frac{d}{dz}\left(\frac{1}{k_0}\underline{D}_H \frac{d}{dz}\mathbf{E}\right) + k_0 \underline{D}_E \mathbf{E} = 0, \tag{3}$$

where

$$\underline{D}_H = \begin{bmatrix} 0 & \left(\frac{k_x^2}{k_0^2}\frac{1}{\varepsilon_{\perp}} - 1\right) \\ 1 & 0 \end{bmatrix}^{-1}, \tag{4}$$

$$\underline{D}_E = \begin{bmatrix} \delta \sin 2(\beta z + \alpha) & [(\varepsilon - \delta \cos 2(\beta z + \alpha)) - k_x^2/k_0^2] \\ -[\varepsilon + \delta \cos 2(\beta z + \alpha)] & -\delta \sin 2(\beta z + \alpha) \end{bmatrix}. \tag{5}$$

Here HTP is defined as $\beta = 2\pi/P(z)$, α is used for the phase jump of the twist defect, and the z axis is the helical axis in the right-handed coordinate system. For the incident light with wavelength λ at an oblique angle θ relative to the z axis, the wave number is $k_0 = 2\pi/\lambda$ and its component in the x direction is $k_x = k_0 \sin\theta$.

The main parameters used in this study are as follows. The indices of refraction parallel and perpendicular to the nematic director are chosen to be $n_{\parallel} = 1.7$ and $n_{\perp} = 1.5$, and the sample is nearly index matched to its surroundings with $n_s = \sqrt{(n_{\parallel}^2 + n_{\perp}^2)/2}$. The smallest and the largest pitches are taken to be $P_{\min} = 320$ nm and $P_{\max} = 380$ nm for the adjustment of the reflection band to cover the range between the wavelengths of 500 and 700 nm. Galerkin's method is applied on Eq. (3) to obtain the matrix equations of the FEM

[20]. For achieving higher accuracy without increasing the number of nodes, second-order elements are used for the basis elements. In order to decompose the forward and backward propagating waves into right and left circularly polarized components, the spectral elements [23] are also used for the consideration of the spatial distribution of energy inside the model. The third-order absorbing boundary condition, which provides better absorption for a plane wave incident at an angle θ, is adopted in the FEM model to truncate the finite element mesh in the scattering problem. The absorption by the medium and the surface roughness at the interface of the two CLC films are neglected.

III. RESULTS AND DISCUSSION

The transmission characteristics of a single CLC film [Fig. 1(a)] with the exponential pitch distribution function (1) are displayed in Fig. 2(a). Without a defect, the transmission spectrum of the simple structure with the thickness $30P_{\min}$ reveals a stop band in the range from 508 to 722 nm (shadow: transmittance under 0.1) for right-handed circularly polarized light. Generally, the reflection bandwidth can be obtained by $\Delta\lambda = n_{\parallel}P_{\max} - n_{\perp}P_{\min}$ because the selective reflection is location-dependent [17]. However, the variation in the reflection bandwidth should also be concerned with the pitch gradient [16,19]. The variation of the reflection wavelength can be expressed as

$$\Delta\lambda_{grad} = \overline{n}\left(\frac{dP(z)}{dz}\right)\Delta z, \tag{6}$$

where $\overline{n} = \sqrt{(n_{\parallel}^2 + n_{\perp}^2)/2}$. Hence the forbidden band will be located between $\lambda_{\min} = n_{\perp}P_{\min}$ and $\lambda_{\max} = n_{\parallel}P_{\max} + \Delta\lambda_{grad}$.

Figure 1(b) shows the model consisting of two CLC films, and the defect is only introduced by a pitch jump in the middle. For normal incident light of right circular polarization (RCP) and left circular polarization (LCP), the transmission spectra of the results for the total thicknesses of $10P_{\min}$, $18P_{\min}$, and $54P_{\min}$ in the stacked structure are presented in Figs. 2(a)–2(c), respectively. In all cases of the transmission spectra for the light of RCP, defect modes are generated by the pitch jump in the forbidden band. It is noticed that the center wavelengths of the defect modes depend on the total thickness of the stacked structure. The peak values and the linewidths of the defect modes also vary according to the thickness of the configuration. In the case of the thickness $10P_{\min}$ [Fig. 2(a)], the peak values of the defect modes almost reach 1, although the structure is insufficient for existence of the defect modes. The minimum value of the full width at half maximum (FWHM) of the defect modes is 9 nm, and the band edges vary slowly. To establish the PBG, a minimum thickness is required in a CLC film [21]. Besides, it is confirmed that the profile of the peak at the defect wavelengths within the PBG depends on the number of periods in a CLC film with a defect [14]. With the thickness $18P_{\min}$ [Fig. 2(b)], localized states appear and the peaks of the defect modes become sharper. Each of the peak values of the defect modes approaches 1 and the minimum of the FWHM is 2 nm. In the previous two cases, no distinct defect

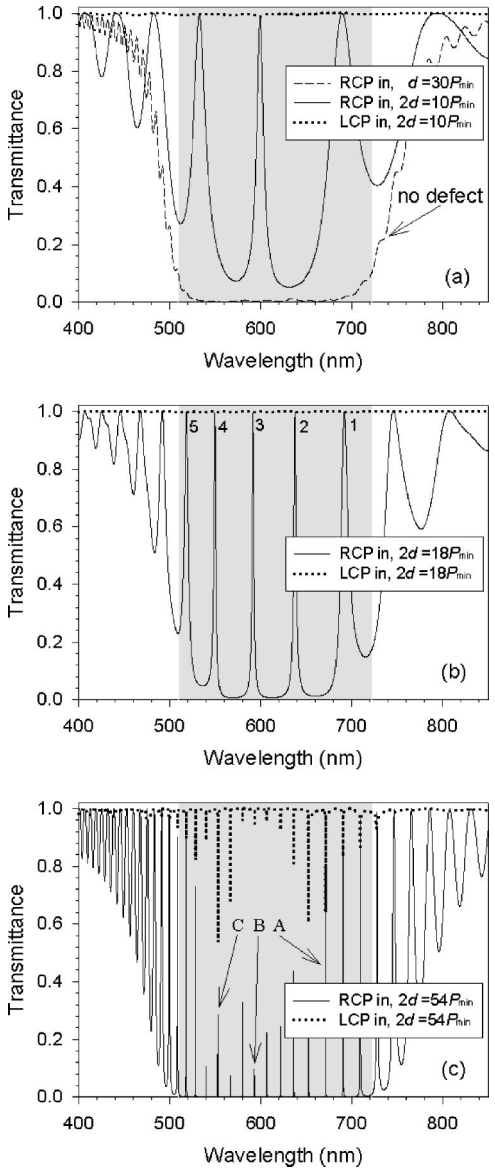

FIG. 2. Transmission spectra of the stacked chiral structure with spatially varying pitch [Fig. 1(b)], which is illuminated by the normal incident light of RCP and LCP. The total thicknesses (a) $2d = 10P_{\min}$, (b) $2d = 18P_{\min}$, and (c) $2d = 54P_{\min}$ are chosen. A forbidden band for a single CLC film with pitch gradient [Fig. 1(a), $d = 30P_{\min}$] is plotted in (a). The shadow in all figures indicates the band gap, which is bounded between 508 and 722 nm.

mode is observed for the incident light of LCP. With the increase of the thickness, the number of the defect modes is larger, and the peaks of the defect modes become sharper. However, when the total thickness is increased to a certain extent, the profile of the peak within a certain range of defect wavelengths for light of RCP is further localized in transmission spectra whereas the peak values are reduced. Furthermore, the sharp dips at the resonance wavelengths appear in the simulated transmittance curve for the incident light of LCP [Fig. 2(c)]. It seems that there is a crossover region where the defect modes can be excited to some proportions by either circularly polarized light [12]. The reasons will be discussed later.

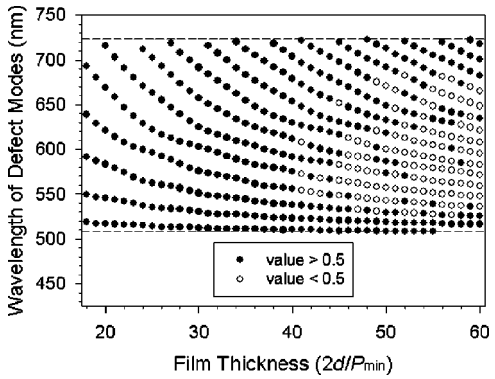

FIG. 3. Thickness dependence of the localized state wavelengths. Closed and open circles represent the peaks of the defect modes for the values beyond and under 0.5, respectively. All of the defect modes are bounded by the upper and lower dashed lines, the same region as the shadow in Fig. 2.

In the stacked structure with a pitch jump, Fig. 3 shows the center wavelengths of the defect modes as a function of the thickness for the incident light of RCP. Closed and open circles represent the peaks of the defect modes for the values beyond and under 0.5, respectively. It was found that the localized modes could be well-confined when the structure thickness is above $18P_{\min}$. As the structure thickness is increased, the number of the defect modes becomes large, and the resonant modes show a blueshift. When the thickness is beyond $40P_{\min}$, the transmittance at some of the defect modes is under 0.5. Further, it seems that the center wavelengths λ_ν of the defect modes existing in the forbidden gap satisfy the relation

$$\frac{1}{\lambda_{\nu+1}} - \frac{1}{\lambda_\nu} = \frac{1}{2\bar{n}\Delta d_\nu \cos\theta} \tag{7}$$

for $\nu=1,2,\ldots,m-1$, where $\lambda_\nu > \lambda_{\nu+1}$, $\theta=0$ for the normal incident light, and Δd_ν is the thickness of an index-matching layer. The transmission characteristics in the PBG are similar to those of a conventional Fabry-Pérot interferometer [24]. However, the conventional spreading of light between two mirrors is generated by the reflection of oblique components of light, and two orthogonal linear polarizations are allowed as resonant modes. In the stacked CLC films, photonic band structures result in the enhanced spreading of light with normal wave-vector components, and the resonance takes place in the resonator only for the light with the same handedness as the CLC helix [25,26]. A schematic drawing of the stacked CLC films shown in Fig. 4 can be used to describe the Fabry-Pérot resonator. P_ν^{eq} could be defined as a local equivalent pitch, and the significant reflection of the two mirrors (M_ν and M_ν^*) occurs over the band

$$\frac{\lambda_0}{n_\parallel} \leqslant \lambda \leqslant \frac{\lambda_0}{n_\perp}, \tag{8}$$

where $\lambda_0=\bar{n}P_\nu^{eq}$. The slice placed between the mirrors can serve as an index-matching layer. Besides, the difference of the particular center wavelengths can be regarded as the free spectral range (FSR)

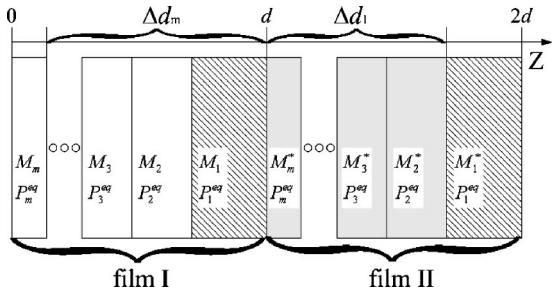

FIG. 4. Schematic drawing of a layered PBG medium, which is constructed by stacking two CLC films with spatially varying pitch. A Fabry-Pérot resonator consists of a pair of CLC mirrors (M_1 and M_1^*) with a local equivalent pitch P_1^{eq} and an index-matching layer (the gray region, thickness Δd_1) sandwiched by the mirrors.

$$\lambda_\nu - \lambda_{\nu+1} = (\Delta\lambda_\nu)_{FSR} \approx \frac{\lambda_\nu^2}{2\bar{n}\Delta d_\nu}, \tag{9}$$

where $\Delta d_\nu \approx d$ and $\Delta d_1 < \Delta d_2 < \cdots < \Delta d_m$. For the defect wavelengths in Fig. 2(b), the values of the FSR calculated via Eq. (9) are about 52, 44, 38, and 33 nm. These values are close to the results of the transmission spectrum shown in Fig. 2(b).

For excitation at the resonance wavelengths shown in Fig. 2(b), the spatial dependence of the relative energy density of the defect modes is sketched in Fig. 5. The distribution of the energy density for the different defect modes corresponds to a relative position of a resonator cavity sandwiched by two CLC films as shown in Fig. 4. For the cavity constructed by the mirrors with the larger (smaller) equivalent pitch, the selective reflection according to Eq. (8) occurs, and the standing wave is strongly peaked at the rear (front) side of

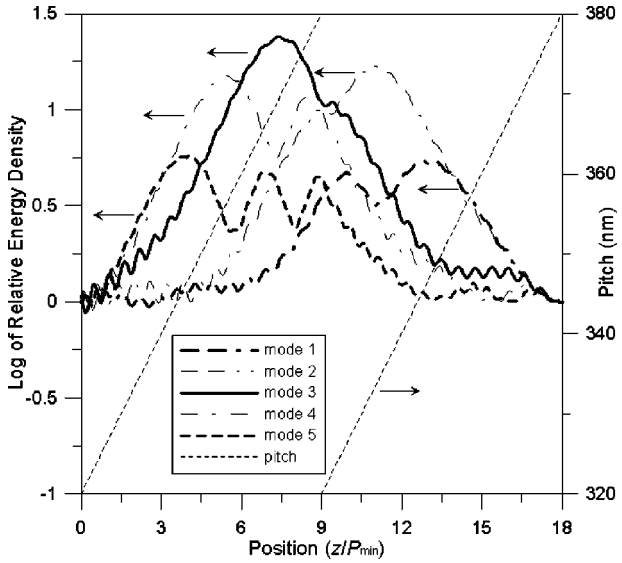

FIG. 5. Distribution of the relative energy density (the common logarithm with base 10) and the pitch inside the stacked chrial structure for the numbered defect modes shown in Fig. 2(b). The center wavelengths of the localized modes are 693 (mode 1), 639 (mode 2), 592 (mode 3), 550 (mode 4), and 519 nm (mode 5), respectively.

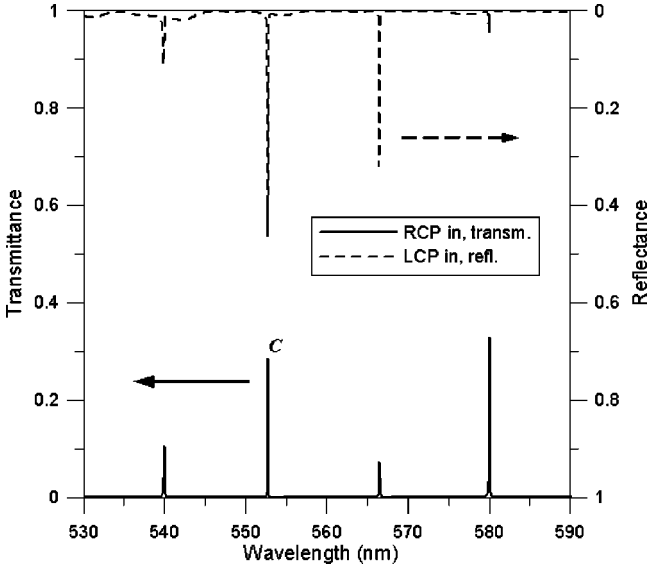

FIG. 6. Transmission and reflection spectra of the stacked chiral structure in the case of Fig. 2(c), which is illuminated by the normal incident light of RCP and LCP. The alphabet C indicates the same defect mode in Fig. 2(c).

the configuration from the location of the light source. Therefore the energy of mode 1 and 2 with the longer defect wavelength is stored mainly at the right side of the defect plane, and that of mode 4 and 5 with the shorter defect wavelength is stored mostly at the left. In addition, it seems that the resonance for all defect modes generates a peak of the energy density near the defect plane. For mode 3, the intensity enhancement can be greater than 20, and the resonant Q factor is more than 250. Due to the band gap in the double composite CLC film shared by the multiple states and the shallow depth of the gap in a local Fabry-Pérot resonator, the enhancement and the factor are relatively less than those in the chiral twist defect created by the discontinuity of the helix in a cholesteric structure [12].

It was found that the dips in the curve of the transmission spectrum for the light of LCP occur when the total thickness of the model is above $28P_{\min}$. The growth of the dips at defect wavelengths becomes more significant for the thickness beyond $40P_{\min}$, and the reduction of the peaks in transmission for the light of RCP is also obvious. The crossover region could be located near the thickness $40P_{\min}$. An anomalous crossover behavior of polarization state in propagation is described by Kopp and Genack for the chiral twist defect produced in the cholesteric structure with constant pitch [12]. At the crossover region, the defect mode can be excited by both circularly polarized waves, and the sum of transmission of RCP wave and reflection of LCP wave is equal to unity. The reason can be explained by the incident light suffering the change of handedness to result in the coupling of the wave to a localized defect mode. For the Fabry-Pérot model which is formed by a pair of identical chiral mirrors with constant pitch [27], the cross-polarized effects are equal as the mirrors look identical when viewed from the inside layer. Therefore the sum of all transmittance of RCP waves and reflectance of LCP waves is approximately equal

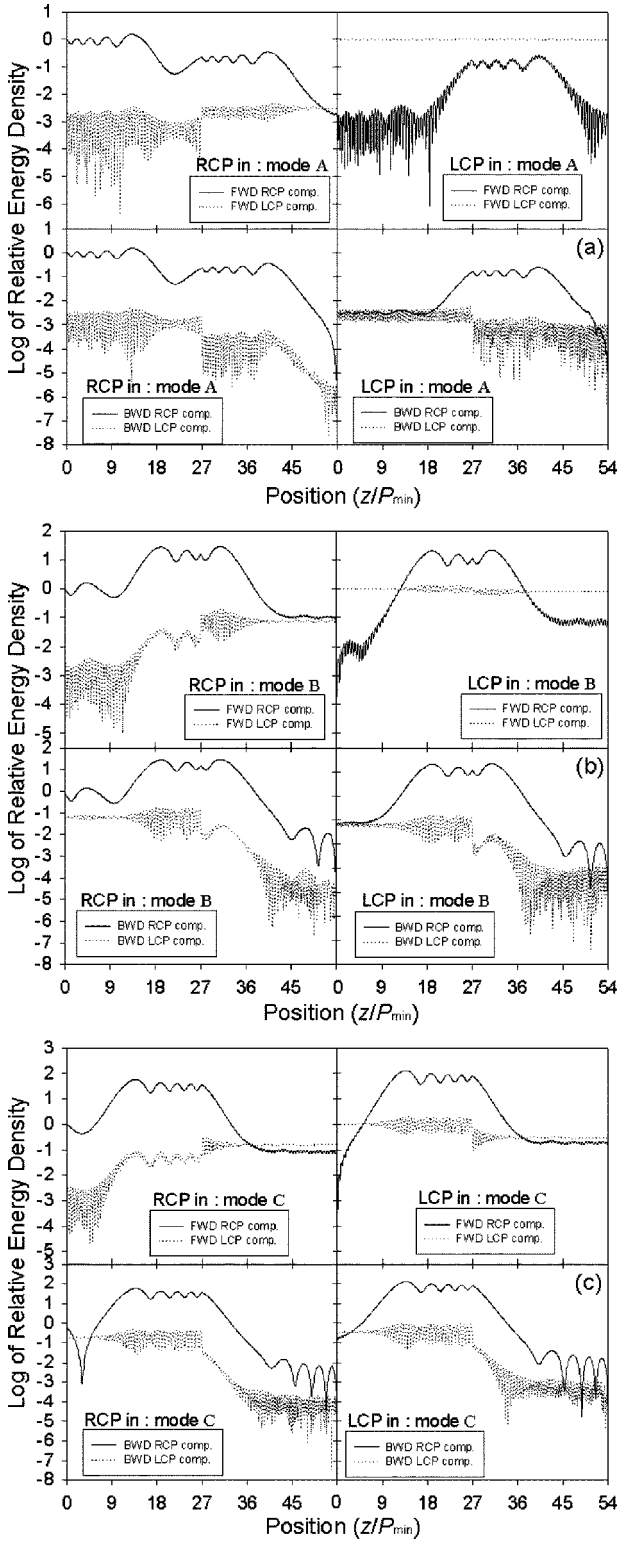

FIG. 7. Distribution of the relative energy density (the logarithm with base 10) inside the stacked chiral structure. Decomposition of the forward and backward propagating waves into right and left circularly polarized components for incident waves of RCP and LCP is shown for the three defect modes in Fig. 2(c). The center wavelengths of the localized modes are (a) 672 nm (mode A), (b) 593 nm (mode B), and (c) 553 nm (mode C), respectively. The top parts of all figures are for the forward waves and the bottom parts of those are for the backward waves.

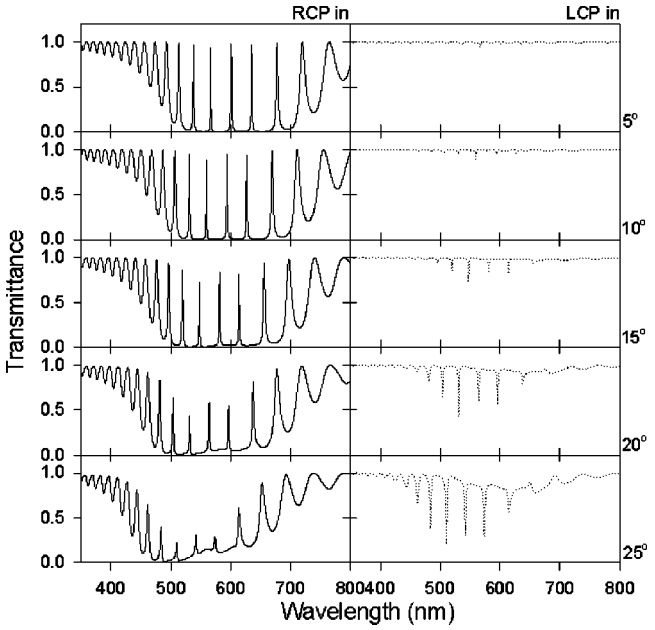

FIG. 8. Transmission spectra of the stacked chiral structure with spatially varying pitch [Fig. 1(b)], which is illuminated by incident waves of RCP and LCP at an oblique angle from 5° to 25°. The structure thickness for simulations is $2d=23P_{\min}$.

to unity at the crossover region. However, the sum is not equal to unity in Fig. 6 from the case of Fig. 2(c). For a local Fabry-Pérot resonator as shown in Fig. 4, the mirrors with different pitch gradient directions look unequal when viewed from the inside layer, even if the mirrors are regarded as the cholesterics with an equivalent constant pitch in the previous statement in explanation of the resonator. In addition, the sandwiched index-matching layer which also has a gradient pitch is not isotropic so that the sum will not equal unity.

In order to examine the polarization of the resonant modes and the defect modes, the waves inside the medium for the three modes in Fig. 2(c) are decomposed into two circularly polarized components with respect to the incident light of RCP and LCP. For each mode, the relative energy density of the light components propagating in the forward (FWD) and backward (BWD) directions is displayed in Fig. 7. This makes it possible to understand the way in which the transmittance is related to the excitation of the resonant state and the coupling between the two circularly polarized waves. In all parts of Fig. 7, the polarization of the exciting modes is the same handedness as the CLC screw for both of the incident RCP and LCP waves. Near the defect plane, a peak of the energy density is generated for all RCP components, and the coupling between the RCP and LCP components would occur. In the case of mode A [transmittance 0.66 for RCP incidence in Fig. 2(c)] shown in Fig. 7(a), the incident RCP wave hardly reaches the resonator cavity with respect to its eigenmode, so that the excitation is small. Strong reflection and weak transmission appear even though the FWD LCP component coupled slightly from the RCP wave at the defect can pass through the structure. Besides, the incident LCP wave is coupled to the RCP components, but the excitation of the components is not strong. Hence it gives rise to the

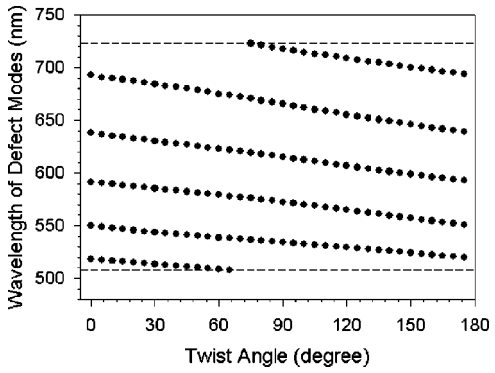

FIG. 9. Dependence of the localized state wavelength on the twist angle for the configuration shown in Fig. 1(c) when the thickness is taken as $2d=18P_{\min}$. All of the defect modes are bounded by the upper and lower dashed lines, the same region as the shadow in Fig. 2.

drop in transmission of the LCP wave. In the case of mode C [Fig. 7(c)], the incident RCP wave can easily reach the resonator to excite the localized mode. Nevertheless, the intensity of the FWD RCP component falling from the defect plane decays greatly to the rear side, and the contribution of the FWD LCP component coupled from the RCP wave is insufficient. The reduction of the transmittance for the incident RCP light appears. For the incident LCP light, the exciting FWD RCP component coupled via the defect also decays rapidly along the z direction, so that the total transmission is reduced. In the case of mode B [Fig. 7(b)], the coupling effect and the energy decay correlated with the thickness are also the same causes of the essential transmission of the incident RCP and LCP waves.

The transmission spectra of the incident RCP (solid line) and LCP (dotted line) waves are shown in Fig. 8 for the different incident angles. The characteristics of the employed structure as shown in Fig. 2(b) are computed for the total thickness $23P_{\min}$. It was found that the localized states introduced into the band gap are not well-confined for the incident RCP wave when the oblique angle is above 15°. In addition, the dips in the transmittance curves of the incident LCP wave are more apparent above this angle. The coupling between RCP and LCP waves is the dominant to destroy the complete transmission when the wavelength reaches the Mauguin limit [21,28]. In oblique angle incidence, the PBG shows a blueshift and so do the corresponding defect modes. The photonic band structures still hold the enhanced spreading of light with near-normal wave-vector components (in the case: $\theta<15°$), and the defect modes in the stop band also satisfy the relation of Eq. (7).

In the model with the defect of a combination of a pitch jump and a phase jump [Fig. 1(c)], Fig. 9 shows the twist angle dependence of the center wavelengths corresponding to the defect modes for the incident RCP light. The horizontal axis indicates the twist angle of the phase jump, and the total thickness of the stacked films in the simulation is $18P_{\min}$. To make a comparison with Ref. [14], in which the phase jump is introduced into the middle of the CLC film with constant pitch, the defect wavelengths from the long to the short wavelength band edge are also tuned by varying the

chiral twist angle from 0° to 180°. The transmittance of the defect modes for all angles is close to 1. It appears that a linear response is present between the defect wavelengths and the twist angle. The feature could be extended to the application of tunable filters. For example, an optical fiber multiple-wavelength filter based on a one-dimensional PBG structure with defects reported by Villar *et al.* can be tuned by changing the refractive index of the defect layers consisting of liquid crystals with the applied voltage [29]. However, the complicated layer stacking and the nonlinearity with respect to the shift in frequency [30] are not easy to control the defect states. The linearity in connection with the shift in wavelength is the benefit of the stacked chiral structure with the double defects. Moreover, one should keep in mind that the purity of polarization for the defect modes will be destroyed at the crossover region.

IV. CONCLUSIONS

The effects of the defects introduced by a pitch jump and a phase jump in a stacked CLC structure with spatially varying pitch have been studied by using the FEM. By means of the introduction of a pitch jump, the dependence of the defect modes on the structure parameters is discussed. The model consists of multiple CLC mirrors with a spatially varying periodic stratified texture that serve as optical resonators to trap optical waves with the modes of the resonators. The energy intensity at the defect site inside the sample can be significantly enhanced by the induced pitch jump to reach a local maximum even if the adjunct coupling between two orthogonally circularly polarized waves gives rise to a slight loss in optical resonators. The loss is not obvious until the total thickness of the stacked films is beyond a critical value. Due to the coupling, the variation with the thickness of the double composite film shows a crossover behavior in the transmission of circularly polarized waves. Furthermore, the transmission feature in a PBG is similar to that in a conventional Fabry-Pérot interferometer. It is also demonstrated that the center wavelengths of the defect modes created by an additional phase jump introduced into the stacked structure with the defect of a pitch jump can be controlled by the twist angle. There is no need for a complex manufacturing procedure to introduce the defects of a pitch jump and a phase jump by stacking the CLC films. The characteristics of the tuning between the defect modes and the twist angle could possess a linear relation and may be useful in the implementation of tunable filters or optical switches of PBG applications.

ACKNOWLEDGMENTS

The authors are indebted to the National Science Council (NSC) of Taiwan for financial support under Contract No. NSC 93-2218-E-006-082.

[1] J. D. Joannopoulos, R. D. Meade, and J. N. Winn, *Photonic Crystals: Modeling the Flow of Light* (Princeton University Press, Princeton, NJ, 1995).
[2] E. Yablonovitch *et al.*, Phys. Rev. Lett. **67**, 3380 (1991).
[3] D. R. Smith *et al.*, J. Opt. Soc. Am. B **10**, 314 (1993).
[4] S. Noda *et al.*, IEEE J. Quantum Electron. **38**, 726 (2002).
[5] M. H. Song *et al.*, Adv. Mater. (Weinheim, Ger.) **16**, 779 (2004).
[6] P. Yeh and C. Gu, *Optics of Liquid Crystal Displays* (Wiley, New York, 1999).
[7] J. P. Dowling, M. Scalora, M. J. Bloemer, and C. M. Bowden, J. Appl. Phys. **75**, 1896 (1994).
[8] K.-C. Shin *et al.*, Jpn. J. Appl. Phys., Part 1 **43**, 631 (2004).
[9] L. M. Blinov and V. G. Chigrinov, *Electro-Optic Effects in Liquid Crystal Materials* (Springer, New York, 1994).
[10] S. Furumi, S. Yokoyama, A. Otomo, and S. Mashiko, Appl. Phys. Lett. **84**, 2491 (2004).
[11] Y.-C. Yang *et al.*, Phys. Rev. E **60**, 6852 (1999).
[12] V. I. Kopp and A. Z. Genack, Phys. Rev. Lett. **89**, 033901 (2002).
[13] M. Ozaki, R. Ozaki, T. Matsui, and K. Yoshino, Jpn. J. Appl. Phys., Part 2 **42**, L472 (2003).
[14] J. Schmidtke and W. Stille, Eur. Phys. J. E **12**, 553 (2003).
[15] T. Matsui, M. Ozaki, and K. Yoshino, Phys. Rev. E **69**, 061715 (2004).
[16] J.-Y. Chen and L.-W. Chen, Physica B **357**, 282 (2005).
[17] D. J. Broer, G. N. Mol, J. A. M. M. van Haaren, and J. Lub, Adv. Mater. (Weinheim, Ger.) **11**, 573 (1999).
[18] M. Mitov, A. Boudet, and P. Sopéna, Eur. Phys. J. B **9**, 327 (1999).
[19] Z. Lu *et al.*, Mol. Cryst. Liq. Cryst. Sci. Technol., Sect. Aol. Cryst. Liq. Cryst. **301**, 237 (1997).
[20] J. Jin, *The Finite Element Method in Electromagnetics* (Wiley, New York, 2002).
[21] Q. Hong, T. X. Wu, and S.-T. Wu, Liq. Cryst. **30**, 367 (2003).
[22] D. W. Berreman, J. Opt. Soc. Am. **63**, 1374 (1973).
[23] O. Z. Mehdizadeh and M. Paraschivoiu, J. Comput. Phys. **189**, 111 (2003).
[24] A. Yariv, *Optical Electronics in Modern Communications* (Oxford University Press, New York, 1997).
[25] J. E. Stockley, G. D. Sharp, and K. M. Johnson, Opt. Lett. **24**, 55 (1999).
[26] V. I. Kopp, Z.-Q. Zhang, and A. Z. Genack, Phys. Rev. Lett. **86**, 1753 (2001).
[27] I. J. Hodgkinson *et al.*, Phys. Rev. Lett. **91**, 223903 (2003).
[28] P. G. de Gennes and J. Prost, *The Physics of Liquid Crystals* (Oxford University Press, Oxford, 1993).
[29] I. D. Villar, I. R. Matías, and F. J. Arregui, J. Lightwave Technol. **22**, 1615 (2004).
[30] I. D. Villar, I. R. Matías, and F. J. Arregui, Opt. Express **11**, 430 (2003).